Chenier Formation Through Wave Winnowing and Tidal Transport

Silke A.J. Tas[1], D.S. van Maren[1,2,3], and Ad J.H.M. Reniers[1]

[1]Faculty of Civil Engineering and Geosciences, Delft University of Technology, Stevinweg 1, Delft 2628 CN, the Netherlands

[2]State Key Lab of Estuarine and Coastal Research, East China Normal University, 500 Dongchuan Rd, Shanghai 200062, China

[3]Deltares, P.O. Box 177, Delft 2600 MH, the Netherlands

Key Points:

- Cheniers develop in three phases: (1) a winnowing phase, (2) an onshore sand transport phase and (3) a crest formation phase
- The main mechanism driving onshore sand transport is wave asymmetry
- Chenier formation through wave winnowing does not require extreme storm conditions

Corresponding author: Silke Tas, s.a.j.tas@tudelft.nl

Abstract

Cheniers are ridges consisting of coarse-grained sediments, resting on top of the fine sediment that forms the otherwise muddy coast. In this paper, we use Delft3D to explore how cheniers are formed through wave winnowing. We identify three phases of chenier development: (1) a winnowing phase, during which mud is washed out of the seabed initially consisting of a mixture of sand and mud, (2) a sand transport phase, when the sand in the upper layer is transported onshore, and (3) a crest formation phase, during which a chenier crest rapidly develops at the landward limit of onshore sediment transport. The main mechanism driving onshore sand transport is wave asymmetry. During calm conditions, sand transport takes place within a narrow band limiting the volume of sand delivered nearshore, and therefore no chenier develops. In contrast, average storm conditions mobilise sufficient sand for a crest to develop. Our results thus reveal that chenier formation through wave winnowing does not require extreme storm conditions. Furthermore, our study showed that chenier formation through wave winnowing is a relatively slow process, with the largest time scales associated with the winnowing and sand transport. Once sufficient sand is available nearshore, the crest develops rapidly.

Plain Language Summary

Cheniers are bodies of sand, observed along muddy coasts. Many muddy coasts worldwide suffer from erosion, but the presence of cheniers helps stabilizing the coastline and protect it against erosion. In this paper, we investigate how waves and tides create a chenier out of a mixed sand-mud bed. First, fine mud is washed out of the bed by waves, and the heavier sand grains are left behind. Then, sand is transported towards the coastline by waves. Finally, the sand accumulates in one location and a chenier is formed. Our results reveal that chenier formation does not require extreme storm conditions, but may already occur at average storm conditions. Furthermore, the first two phases (washing out the mud and transporting the sand) are relatively slow, but once sufficient sand is available nearshore, the chenier will form rapidly. The results of this study help to understand how, where and when cheniers may develop, which helps to predict the fate of (eroding) muddy coasts.

1 Introduction

Cheniers are ridges consisting of wave-reworked coarse-grained sediments, resting on top of muddy sediment (Augustinus, 1989; Otvos & Price, 1979). Cheniers may occur as a single ridge (e.g. in Demak, Indonesia) or they may be part of a chenier plain (e.g. in Louisiana, USA), where multiple clusters of cheniers, separated by mudflats, are observed. Chenier coastlines consist of mostly very fine sediments, with a small fraction of coarser grained particles, which can have a marine or fluvial origin. For example, the chenier sediment in Tourville Bay, Australia is of local, marine origin (Belperio et al., 1988) while sand in the cheniers in French Guiana originates from sand supplied by local rivers rather than from the mud banks migrating alongshore (Prost, 1989; Pujos et al., 2001; Anthony et al., 2010). Cheniers can be formed in two ways, which are related to the origin of the coarser (sandy) sediments (Augustinus, 1989). Sand can originate from winnowing, where mud is brought into suspension and the remaining sand is transported onshore through wave-driven sediment transport, accumulating in a sandy ridge. Alternatively, cheniers may develop from spits forming downdrift of river mouths. In this paper, we will focus on the first mechanism: chenier formation through wave winnowing.

Winnowing requires sufficient wave energy, for example during a storm event (Woodroffe & Grime, 1999) or during a period of increased wave action (e.g. during inter-mudbank phases along the coast of the Guianas (Anthony et al., 2010)). Furthermore, sufficient coarser-grained particles need to be available in the nearshore zone where waves create sufficiently high bed shear stresses to suspend the fines and mobilise the coarser sediments. For example, in the Louisiana Chenier Plain, cheniers are formed near the mouths of rivers discharging high fluvial sediment loads (Rosen & Xu, 2011). When higher waves coincide with spring tides, both elements (wave energy and sediment availability) are reinforced, as the waves may now rework sediments that were not available during normal conditions, e.g. the chenier formation in the Firth of Thames (Woodroffe et al., 1983; Dougherty & Dickson, 2012).

The objective of this paper is to understand how cheniers are formed through wave-induced winnowing. Despite the large amount of studies on cheniers (as in the references above) their formation is largely described in a qualitative sense, and a systematic study into chenier formation in response to wave and tidal processes is lacking. A first step towards a quantitative approach of chenier formation was made by Nardin and Fagherazzi

(2018), who studied the development of entire chenier plains using Delft3D. In this paper, we focus on the development of a single chenier, hence looking at much smaller spatial and temporal scales. We therefore deploy a process-based numerical model (Delft3D) to identify the responsible processes and mechanisms during the various phases of chenier genesis, and determine under which conditions a chenier develops. In Section 2.1 we provide an overview of the relevant sediment transport formulae and how they are implemented in Delft3D. Section 2.2 gives a brief overview of the model set-up, which is based on the model developed by Tas et al. (2022) through validation against field observations (Tas et al., 2020). We explore chenier development through a number of (idealised) scenarios described in Section 2.3. These scenarios reveal three phases of chenier formation which are presented in Section 3. The implications of our findings, as well as some limitations of our approach are discussed in Section 4 and the conclusions are presented in Section 5.

2 Methods

The formation of cheniers through wave-induced winnowing is explored using a Delft3D-FLOW morphodynamic model in combination with a SWAN wave model. Delft3D-FLOW solves the unsteady shallow water equations in two (depth-averaged) or three dimensions (Lesser et al., 2004) and SWAN is a third generation numerical wave model (Booij et al., 1999). Below (and in Appendix Appendix A) we summarize the relevant sediment transport formulae that are used to calculate sediment transport in Delft3D, followed by a description of the model set-up.

2.1 Sediment Transport in Delft3D

We consider two types of sediment: cohesive (mud) and non-cohesive (sand). Sand can be transported as bed load and as suspended load. Sediment transported as bed load is limited to a thin layer above the bed; sand particles higher in the water column are transported as suspended load. Mud is transported as suspended load or as fluid mud (for high concentrations the mud is transported as a viscous layer near the bed). Sediment transport (both sand and mud; both suspended and bed load) requires the exceedance of a critical bed shear stress to initiate movement of the sediment particles.

Bed load transport of sand is calculated using the empirical formula of van Rijn (1993). The suspended sediment transport of both mud and sand by currents are com-

puted with an advection-diffusion equation. Additionally, there is also suspended sand transport due to wave asymmetry, as a result of asymmetric wave orbital velocities, which is approximated following van Rijn et al. (2001). Appendix Appendix A gives an overview of the relevant sediment transport formulae.

2.2 Model Set-Up

We follow a quasi 1D approach: the model is set up in depth-averaged mode and is alongshore uniform. In order to avoid shadow effects, the WAVE-domain is much wider than the FLOW domain. The grid cell size Δx reduces from 25 m at deep water to 1.5 m nearshore. The bed has a constant slope of 1:500 and consists initially of a homogeneous mixture of 2 fractions: mostly mud and a small sand fraction ($D_{50} = 235\mu$m). The mud in Demak is very soft (with a strength of the mud layer being much too low to carry a human). Little is known about the erosion properties of such thick mud bed properties. The most similar conditions for which erosion properties of such thick fluid mud beds have been described in literature are those of van Maren, Winterwerp, and Vroom (2015), using a critical bed shear stress $\tau_{\mathrm{cr,e}} = 0.5$ N/m^2. Settling velocities in similar environments generally range from 0.2 to 5 mm/s (Soulsby et al., 2013; Manning & Dyer, 2007; van Maren, van Kessel, et al., 2015; van Leussen & Cornelisse, 1993). Measurements in Demak suggested a small settling velocity on the lower end of this range (Deltares & BioManCO, 2019), hence we set $w_s = 0.5$ mm/s. The dry bed density is typically around $\rho_{\mathrm{dry}} = 300$ kg/m^3. With all other parameters largely based on observations or earlier work, the last remaining parameter (the erodibility parameter M_{ero}) was calibrated such that the bed was dynamic but still attained dynamic equilibrium, $M_{\mathrm{ero}} = 1.10^{-4}$ kg/m^2/s.

The bed composition is modelled using a layered bed stratigraphy: the bed is composed of multiple layers in order to account for winnowing of mud from the mixed bed. The active upper layer is 2 mm thick and always fully mixed. Upon deposition, sediments settle in the upper layer, leading to migration of sediments from the upper layer to the first bed stratigraphy layer. Only the upper layer is available for erosion, and upon erosion sediment from the first stratigraphy layer migrates to the active layer. The stratigraphy layers have a maximum thickness of 10 cm, except the lowest layer when the maximum of 10 layers is reached (this layer is limited by a non-erodible boundary 1 m below the initial bed level).

At the offshore boundary, a (time-varying) water level and wave height is prescribed (see Section 2.3 hereafter). A delayed transfer of wave energy in the landward direction is computed with a roller model (Svendsen, 1984; Nairn et al., 1991; Reniers et al., 2004). This introduces a time lag (and therefore spatial lag) between the moment of wave breaking and the moment of energy dissipation, which is necessary for realistic modelling of cross-shore profile development of barred beaches (Reniers et al., 2004).

The computational time was reduced by introducing a morphological acceleration factor MorFac (multiplying the bed level change every timestep with MorFac). We have scaled the MorFac with the wave height, using a smaller factor for larger wave heights (hence larger/faster bed level changes) and verified our choice by comparing the model results with a smaller MorFac.

2.3 Model Scenarios

Boundary conditions representing the conditions in Demak, Indonesia are defined in multiple model scenarios, see Table 1. Three wave scenarios are defined: (1) sea breeze-induced waves, representing the energetic conditions during the SE monsoon season; (2) average storm conditions, which occur multiple times per NW monsoon season; and (3) extreme storm conditions, representing a storm with a return period of 10 years. The extreme storm conditions are estimated based on the peak-over-threshold analysis of Alferink (2022) performed on Wave Watch III data, which were validated against field observations. A simple sinusoidal tide is prescribed at the offshore boundary, composed of the largest constituent in Demak, K1 (Tas et al., 2020), with three varying amplitudes representing no tide ($a_{K1} = 0$ m), neap tide ($a_{K1} = 0.25$ m) and spring tide ($a_{K1} = 0.5$ m). The sand fraction in the initial homogeneously mixed sediment bed is varied between 5, 10 and 20%. Each wave scenario is combined with any of the tidal amplitudes and sand fractions (27 scenarios). These idealised scenarios are supplemented with one scenario forced with a realistic time series for water levels and wave conditions at the offshore boundary (see Section 3.6).

3 Results

Figure 1 shows the formation of a chenier under constant wave conditions representing average storm conditions ($H_s = 1.3$ m and $T_p = 5.6$ s, see Table 1), in the absence of tide (constant water level), starting from a fully mixed bed with 10% sand. The

Table 1. Wave conditions for the three wave scenarios

Wave conditions	H_s [m]	T_p [s]	MorFac
Sea breeze	0.6	3.5	100
Average storm	1.3	5.6	25
Extreme storm	2.47	7.7	7.5

chenier develops in three phases: (1) winnowing, during which mud is washed out and the upper layer of the bed becomes increasingly sandy; (2) the sand in the upper layer is transported landward; and (3) crest formation, essentially the abrupt heightening of the chenier crest when sufficient sediment is available. During phase 1 and 2, when a thin sand layer is formed and transported landward, bed level changes are small; most morphodynamic changes take place during phase 3 when the chenier crest develops. The chenier exemplified in Figure 1 reaches its full height after 120 days, after which the speed of bed level changes slow down.

Chenier development is subsequently explored for other wave conditions as well: lower waves (representing an energetic sea breeze-day during the SE monsoon season) and higher waves (representing an extreme storm). The resulting evolution of the sand fraction in the upper layer of the bed (left column, panels 2a, 2d and 2g), bed level changes (middle column, panels 2b, 2e and 2h) and sand transport (right column, panels 2c, 2f and 2i) are given in Figure 2, for extreme storm conditions (upper row), average storm conditions (middle row) and energetic sea breeze conditions (lower row) respectively.

For all wave scenarios, mud is winnowed from the bed and sand is subsequently transported landward, but only for the higher wave scenarios a chenier crest develops (Figures 2b and 2e). The sediment sorting (left column) and sand transport (right column) exhibit similar trends, which suggests that onshore sand transport depends on sand availability, which is a direct result of winnowing. This landward transported sand culminates close to the shoreline and, for the higher wave conditions, develops into a chenier crest.

3.1 Phase 1: Winnowing

For all wave scenarios, mud is eroded over almost the entire domain (see Figure 3, left y-axis, when $|\tau_{\mathrm{cw,max}}| - \tau_{\mathrm{cr,e}} > 0$). However, the onset of sand transport requires

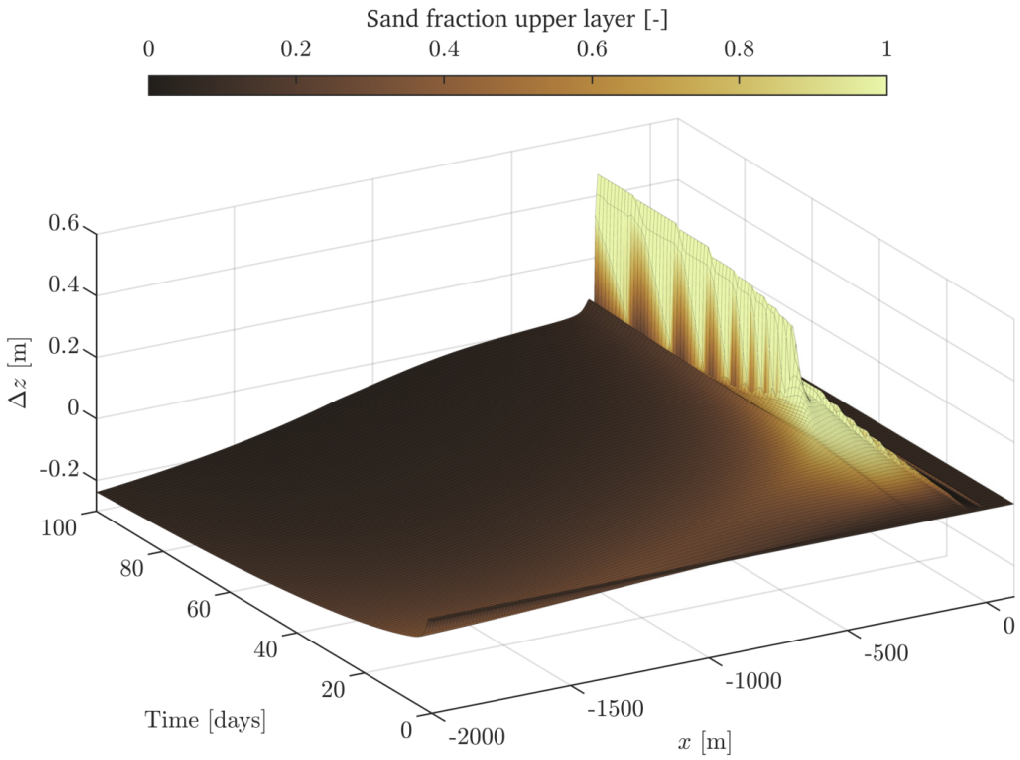

Figure 1. Changes in bed elevation and composition over time. The horizontal axes represent the time and x-coordinate (with the origin of the x-axis corresponding to the shoreline at MSL). The vertical axis represents the elevation change relative to the initial profile, and the colours represent the sand fraction of the upper layer (with 0 only mud and 1 only sand; the sand fraction of the initial mixture was equal to 0.1). The boundary conditions are constant over time, representing average storm conditions ($H_s = 1.3$ m and $T_p = 5.6$ s) and a constant water level.

higher flow velocities (when $|v_{\text{eff}}| - v_{\text{cr}} > 0$, right y-axis in Figure 3). This difference is especially relevant for the sea breeze scenario (Figure 3c), where mud is eroded over a much wider area, while sand is only eroded landward of $x = -900$ m. This means that seaward of $x = -900$ m, mud is being eroded from the upper bed layer, but the sand particles remain immobile, which results in a higher sand fraction in the upper bed layer (visible in Figure 2g). Landward of $x = -900$ m, both sediment fractions are mobilised. For higher waves (see Figures 3a-b), the erosion thresholds for both sediment fractions are exceeded at increasingly deeper water, resulting in erosion of both mud and sand over almost the entire domain.

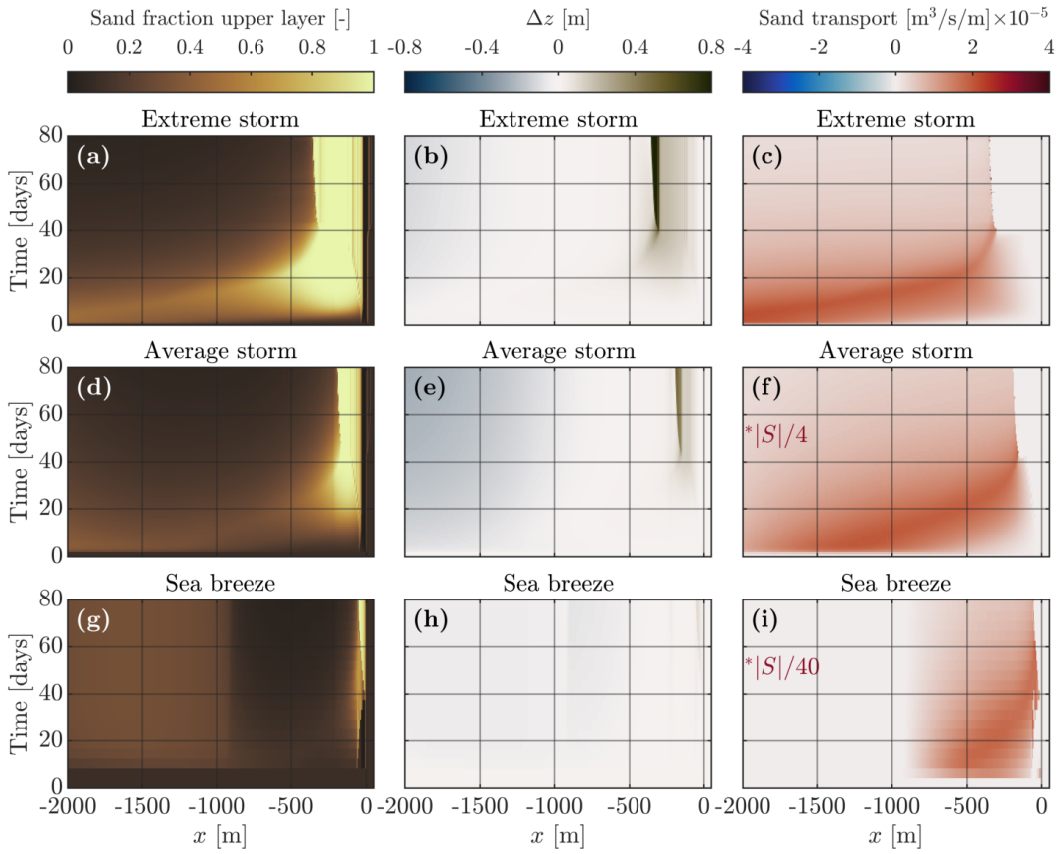

Figure 2. Evolution of the sand fraction in the upper layer (left column), the bed level change (middle column) and the sand transport (right column) for three wave scenarios (extreme storm, average storm, and sea breeze). *In order to visualize the sand transport trends for all scenarios, the colour scale is corrected with a factor 1/4 and 1/40 in panels **(f)** and **(i)**, respectively (i.e. the darkest red represents a a transport of 4.10^{-5} m^3/s/m in **(c)**, 1.10^{-5} m^3/s/m in **(f)** and 1.10^{-6} m^3/s/m in **(i)**).

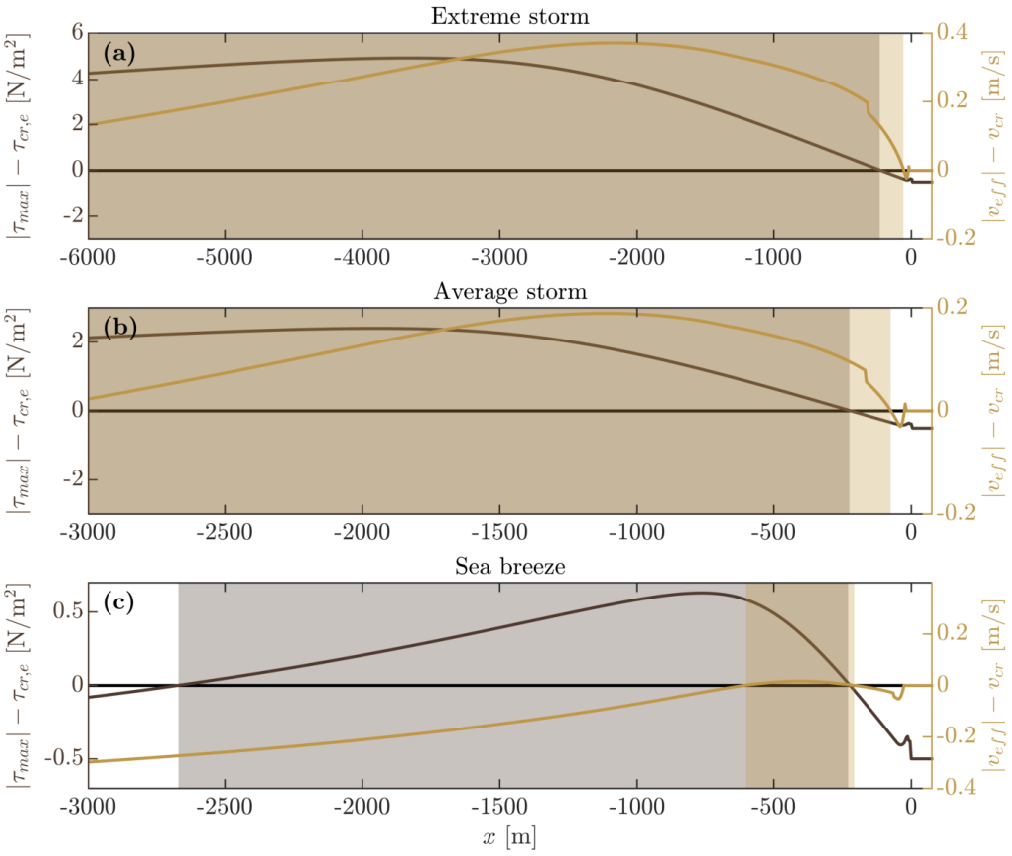

Figure 3. Visualisation of the area where the threshold for the initiation of motion is exceeded for three wave scenarios (panels a-c). Mud (dark brown, left y-axis) is eroded when $|\tau_{cw,max}| - \tau_{cr,e} > 0$ and sand (light brown, right y-axis) is eroded when $|v_{eff}| - v_{cr} > 0$.

3.2 Phase 2: Sand Transport

Sand transport (right column in Figure 2) is directly linked to the availability of sand in the upper layer (left column Figure 2). Sand transport is therefore supply-limited, i.e. not only governed by the transport capacity, but also by the sand availability (and thus winnowing). During phase 2, the main mechanism for onshore sand transport is wave asymmetry, as demonstrated with a simple sensitivity analysis. The modelled onshore sand transport by wave asymmetry can be modified with a user-defined parameter f_{SUSW} (calibrated to 0.5 using field observations, see Tas et al. (2022)). Applying a much lower value ($f_{SUSW} = 0.05$) results in a much lower onshore sand transport (compare panels 4a-c with panels 4d-f), revealing that onshore transport indeed results predominantly from wave asymmetry.

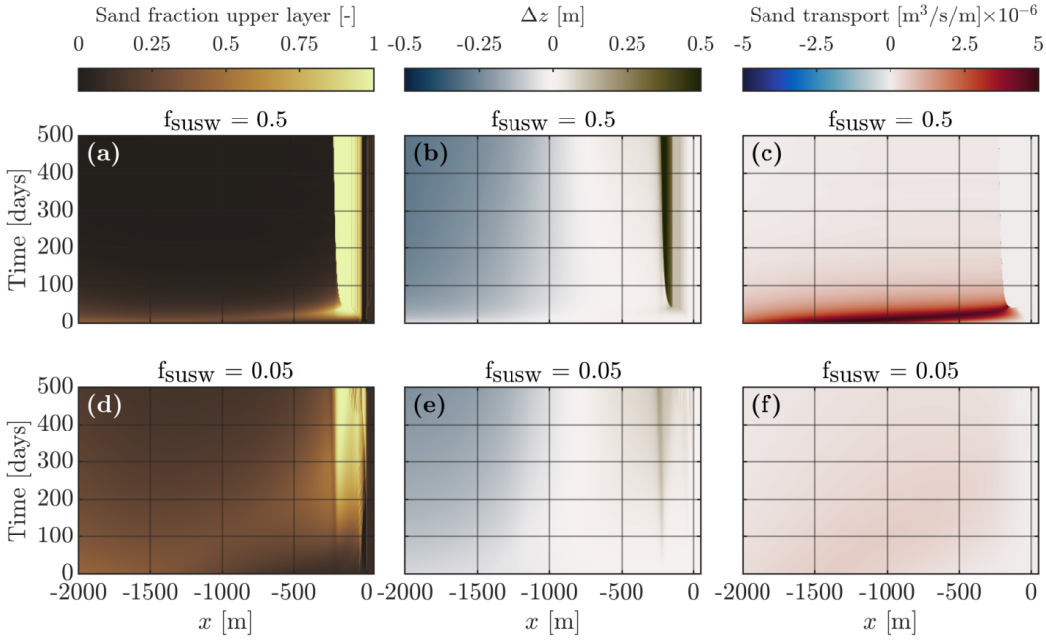

Figure 4. Sand fraction in the upper layer (left column) and total sand transport (right column) for values of $f_{\mathrm{SUSW}} = 0.5$ (upper row) and $f_{\mathrm{SUSW}} = 0.05$ (lower row).

Although there is still some onshore sand transport for the scenario with a ten times smaller value for f_{SUSW} (Figure 4f), leading to a sandy region near the shoreline (Figure 4d), the total volume of onshore sand transport and resulting bathymetric change (Figure 4e) is small.

3.3 Phase 3: Crest Formation

The last phase of chenier formation is rapid sand accumulation at one location, thereby shaping a chenier crest. This process is very fast and abrupt: once a certain threshold is exceeded, the crest height rapidly increases.

Sedimentation (and erosion) can be directly linked to sediment transport gradients. A negative transport gradient is defined as a landward decrease in sediment transport, resulting in sediment deposition. Figure 5 shows the bed level change (left column), the sand transport (middle column) and the sand transport gradient (right column) for a scenario during average storm conditions. The three rows show a different initial sand content, in this section we focus on the middle row (sand content of 10%), the other rows (5% and 20% sand) will be discussed in Section 3.4.

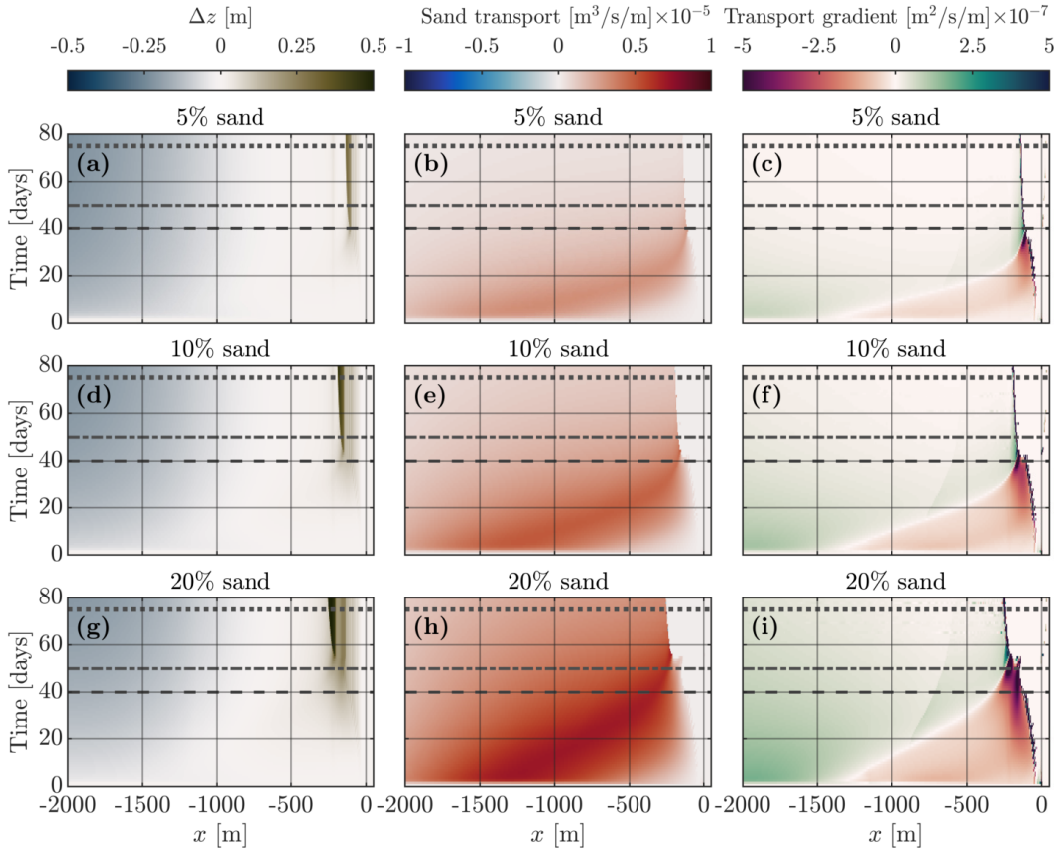

Figure 5. Bed level change (left column), sand transport (middle column) and sand transport gradient (right column) for three different initial sand fractions: 5% (upper row), 10% (middle row) and 20% (lower row). The horizontal dashed lines correspond to the different panels in Figure 6 (dashed line: 40 days, panel 6a; dash-dotted line: 50 days, panel 6b; and dotted line: 75 days, panel 6c).

Initially, sediment transport is maximal in deeper water ($x = 1000-1500$ m with water depth $d = 2-3$ m at $t = 0$ in Figure 5e). Sand is eroded seaward of this sand transport peak (positive transport gradient in Figure 5f) and deposited landward (negative transport gradient). The winnowed sand body migrates landward, driven by wave asymmetry and a gradual depletion of sand in the sand-mud mixture. The moment the peak sand transport rate is close to the shore ($x = 200$ m at $t = 40$ days in Figure 5e), the decrease in transport in landward direction is concentrated over such a narrow zone that a chenier crest emerges (Figure 5d).

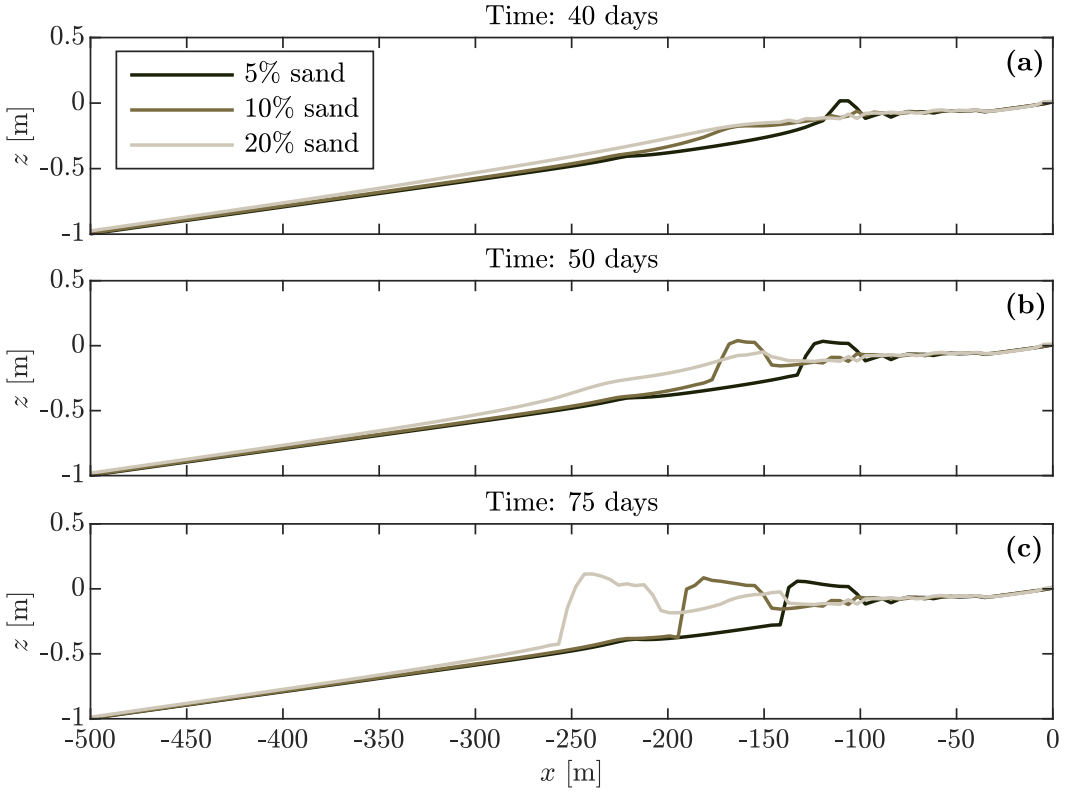

Figure 6. Bed level evolution at three moments in time (panel **(a)** after 40 days, panel **(b)** after 50 days, and panel **(c)** after 75 days) for three different initial sand fractions: 5% (darkest shade brown), 10% (medium shade brown) and 20% (lightest shade brown). The three sand fraction scenarios are the same as in Figure 5.

3.4 Effect of the Initial Sand Fraction

The size of the developed cheniers, but also the time required to develop a chenier, depends not only on the waves (as evaluated above) but also on the sand fraction in the sand-mud mixture. Figure 6 shows the chenier formation process for three different initial sand fractions (different shades of brown) at three points in time (panels a-c, corresponding to the time markers in Figure 5).

Interestingly, the lowest initial sand fraction (darkest line in Figure 6) leads to the fastest emerging chenier. This initially counter-intuitive observation can be explained by sand winnowing. Because of the lower sand content in the bed, the upper bed layers are more quickly depleted of sand, the maximum transport peak converges more rapidly with the shoreline, and as a result crest formation (phase 3) starts earlier. The onset of crest formation for the scenario with 10% sand is visible around $x = -170$ m (Figure

250 6a) and for the scenario with 20% sand around $x = -230$ m (Figure 6b). The chenier
251 crest is located where the fine sand layer (which slowly built out from the water line) con-
252 verges with the steepest transport gradients (see Figures 5c, 5f and 5i).

253 ### 3.5 Effect of Tides

254 The model scenarios evaluated up to now assume a constant water level. In the fol-
255 lowing scenarios a single tidal component (K1, the dominant constituent) is prescribed
256 as boundary condition with an amplitude of 0.5 m (the amplitude of spring tide in De-
257 mak). Chenier formation under average storm conditions and the simplified tide is vi-
sualized in Figure 7.

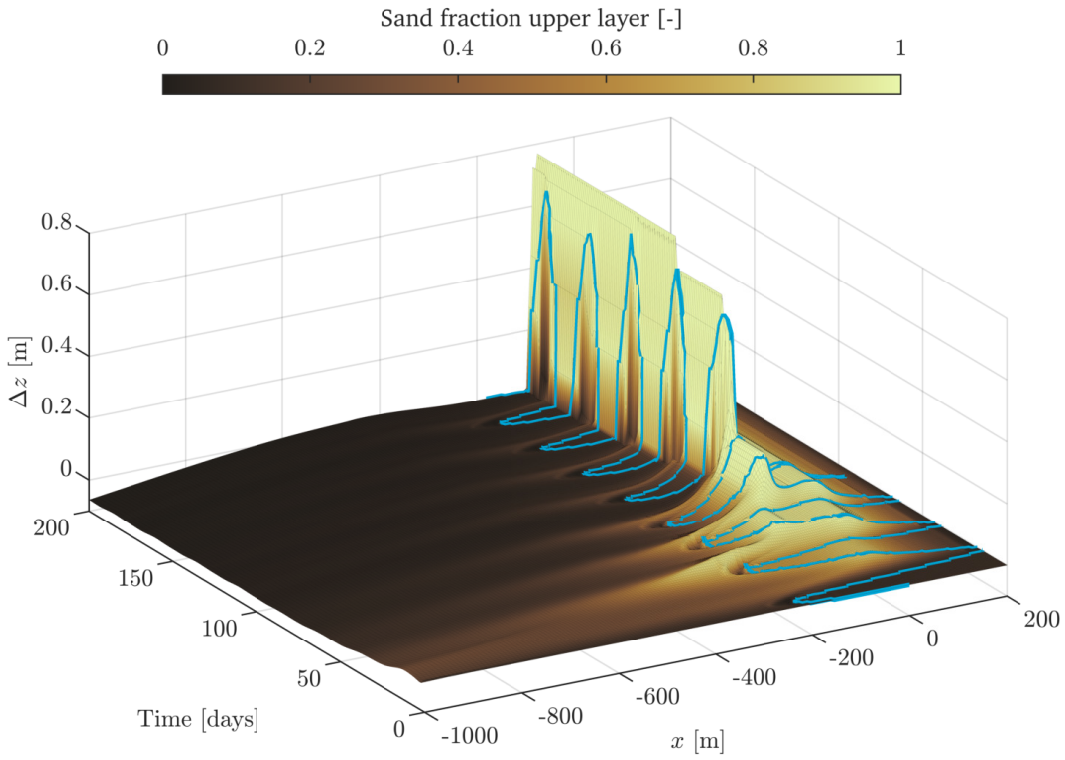

Figure 7. Changes in bed elevation and composition over time. The horizontal axes represent the time and x-coordinate, and the vertical axis the elevation change relative to the initial profile. The colors show the sand fraction of the upper bed layer. At the offshore boundary, a constant wave condition is applied (average storm; $H_s = 1.3$ m and $T_p = 5.6$ s), a simple tidal signal ($a_{K1} = 0.5$ m) and starting from a fully mixed bed with a sand content of 10%. The blue line shows the water line at each time step.

258

The effect of tides on chenier formation can be inferred from Figure 7 (with tides) and Figure 1 (same wave conditions, but constant water level). With tidal forcing, the chenier develops more slowly compared to a simulation without tides (crest formation after 90 days versus 43 days), and the crest is located more landward (around $x = -70$ m versus $x = -155$ m) and higher (around $z = 0.55$ m above MSL versus $z = 0.10$ m above MSL).

This difference is related to the time and spatially varying water depths and bed shear stresses. In the intertidal zone, sand is only transported when the bed is submerged (the migrating water line is indicated with the blue line in Figure 7), and therefore the chenier cannot develop during periods of emergence. This explains the slower development of the chenier under tidal conditions. The height of the chenier crest is limited by two factors: the water surface and the available volume of sand. The maximum water surface is higher for tidal conditions, leading to a higher crest height. But in addition to this, the waves propagate further landward during high tide, thus enlarging the bed surface from which sand can be winnowed (i.e.: more sand is available under tidal conditions, favouring a higher chenier).

3.6 Realistic Boundary Conditions

As a final step, chenier formation under realistic time series for the wave conditions and water levels is evaluated. Wave conditions were derived from the Wave Watch III hindcast data (The WAVEWATCH III Development Group, 2019) for the NW monsoon season between 1 December 2016 and 1 March 2017. The water levels were calculated using all tidal constituents derived from the water level data measured at Semarang (Tas et al., 2020). A morphological factor of 5 was applied to realise bed level changes within acceptable computational periods (Figure 8).

During the first weeks, the wave height is low (rarely exceeding 0.8 m). As a result, sand is only winnowed from a narrow nearshore zone and transported to the coastline (phase 1 and 2), but the amount of sand is insufficient to develop into a crest (phase 3). A fine sand layer develops relatively high in the profile, above MSL.

Winnowing and sand transport occur over a much wider zone during the first storm ($t = 100$ days), and more sand is transported landward. This leads to sufficient nearshore sand availability for the formation of a chenier crest. The crest is formed at the seaward edge of the sand layer, which is relatively far landward.

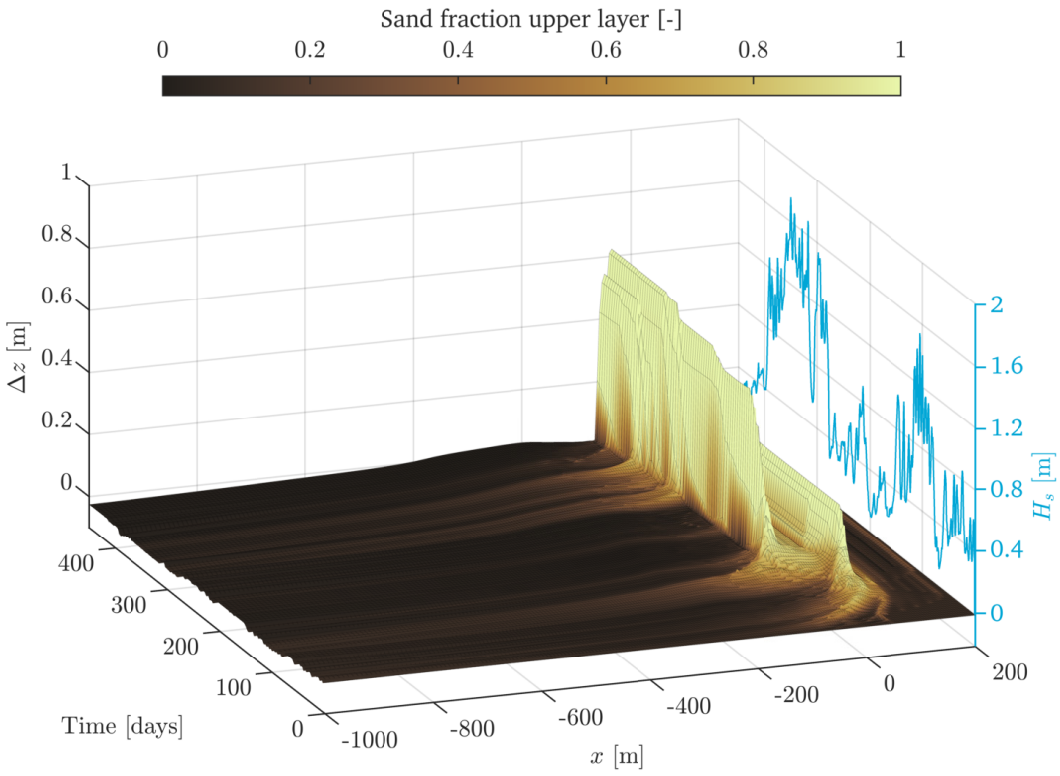

Figure 8. Changes in bed elevation and composition over time. The horizontal axes represent the time and x-coordinate, and the vertical axis the elevation change relative to the initial profile. On a secondary z-axis (blue axis) the significant wave height at the offshore boundary is given. The colors show the sand fraction of the upper bed layer. At the offshore boundary, a time series for the wave conditions and water levels representative for the NW monsoon season were applied.

After a brief period with calmer conditions (during which the chenier remains static although sand is transported landward to form a fine sand sheet seaward of the chenier), a new storm initiates a second phase of substantial onshore sand transport and the formation of a second chenier crest. This crest is again located at the seaward edge of the sand layer, and is thus located more seaward than the first chenier crest. This crest quickly grows in height and shelters the older chenier crest from wave action, until it stabilises with its crest around the highest tidal levels. Later storm periods transport new volumes of sand nearshore, leading to a slight widening of the chenier crest in the seaward direction.

A notable difference between this model scenario with varying boundary conditions and the previous scenarios with constant boundary conditions, is the role of the calmer

periods between storms. The wave energy during these calm periods is too weak to transport sufficient sand nearshore to develop into a chenier crest. However, there is still onshore sand transport. This sand supplied during calm conditions provides the material for rapid chenier formation during stormy periods. Therefore cheniers may more rapidly emerge during storms following a period of relatively calm conditions.

4 Discussion

We have numerically investigated chenier formation for a range of hydrodynamic boundary conditions representing the environmental conditions near Demak, Indonesia (see Table 1). A chenier developed for 18 of the 27 scenarios: the only conditions for which no chenier crest developed were for smaller, sea breeze-induced waves. These various hydrodynamic conditions influence the location where the chenier emerges (x_{crest}) and the time it takes for the chenier to develop (t_{crest}). Figure 9 summarises x_{crest} and t_{crest} for all scenarios with chenier development. Here, the moment of crest formation was defined as the moment the chenier crest reaches 50% of its final crest height, which coincides with the moment of rapid crest heightening (when the highest transport gradients reach the shoreline - see also Figure 5).

The chenier crest develops further offshore for scenarios with higher waves (filled markers) and/or higher initial sand content (yellow markers). Both contribute to a larger sand volume in the nearshore, which allows the initial nearshore sand layer to build out further offshore. A larger tidal range slows down the speed of chenier formation (high t_{crest}), as the varying water levels lead to a larger range in water depths and bed shear stresses. The diagram also provides more details on the role of the initial sediment substrate. The results in section 3.4) suggested that a chenier develops slower for higher sand content but closer inspection of Figure 9 reveals that this is only true for for high wave conditions or in the absence of tide. For moderate wave ($H_{\mathrm{s}} = 1.3$ m) and tide ($a_{\mathrm{K1}} =$ 0.25–0.5 m) conditions (open triangles and squares) the duration of crest formation is independent of the initial sand content.

Chenier formation has always been associated with extreme storms (e.g. Woodroffe and Grime (1999); Dougherty and Dickson (2012)), but our model results suggest that also milder storm conditions are important for chenier formation. This can be explained with the three phases which drive the formation of cheniers: winnowing, onshore transport, and crest formation. Milder storms regularly occurring during the NW monsoon

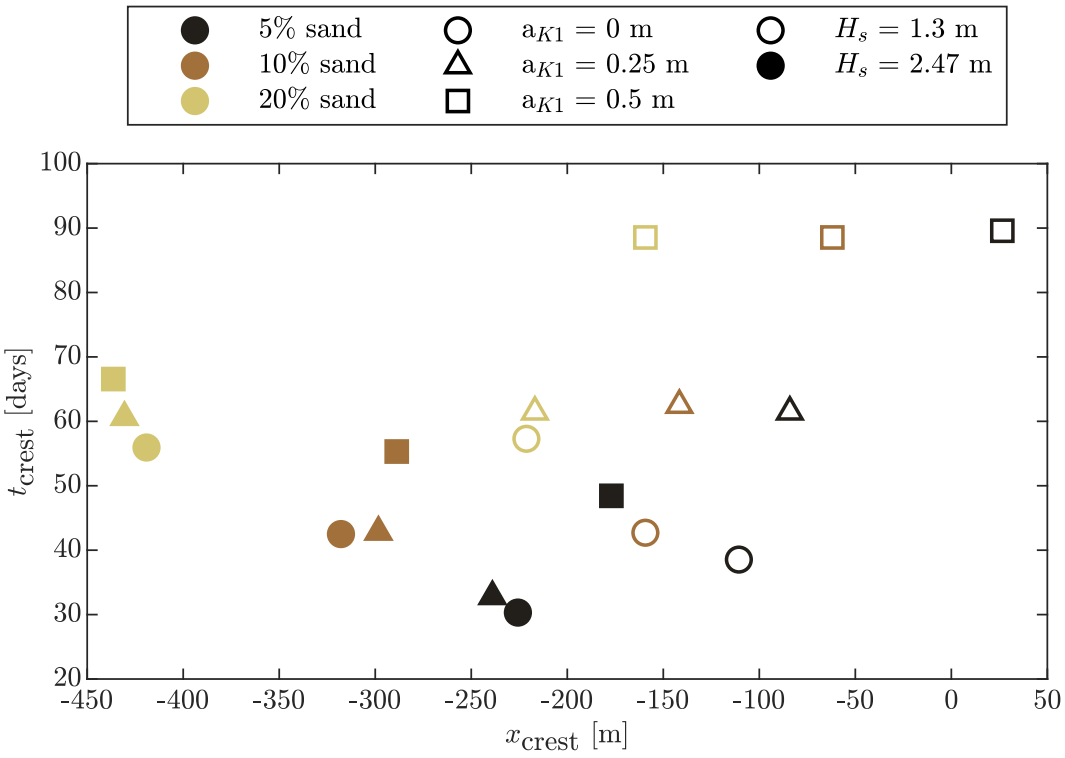

Figure 9. Location of the chenier crest (horizontal axis) and duration until crest development (vertical axis) for all scenarios that resulted in a chenier (18 out of 27 scenarios described in Table 1, excluding the sea breeze wave conditions). The shape of the data points relate to the tidal range (circle: no tide, triangle: neap tide, square: spring tide), the colours represent the sand content of the bed (lighter for higher sand content) and the two wave conditions are distinguished by the fill (no fill: average storm conditions, filled: extreme storm conditions).

season are already energetic enough to activate all three phases of chenier formation. Furthermore, small amounts of sand are still transported nearshore during calmer periods in-between. While the winnowing phase has been described qualitatively in previous work (Augustinus, 1980; Rhodes, 1982; Woodroffe & Grime, 1999; Nardin & Fagherazzi, 2018; Anthony et al., 2019), our findings provide the first quantitative investigation on this winnowing process in relation to the development of individual cheniers.

Our model results further suggest that the largest timescales are associated with phase 1 (winnowing) and 2 (onshore transport). The actual crest formation, however, is very fast (see also Section 3.3). In our model approach the timescales of winnowing are dependent on the state of the initial sediment bed (fully mixed), and therefore it takes a long time for the chenier to develop. It is also not realistic that storm conditions oc-

cur uninterrupted for 50 days (as in our moderate and high storm conditions simulations). However, a sequence of storms (and calmer periods and seasons in between) may eventually set up a sufficiently pre-sorted situation, which could allow a regular, short storm to form a chenier.

The scenario with a realistic time series for the wave conditions and water levels reveal the development of a second chenier crest, seaward of the first crest. This may seem similar to bar systems which often have multiple shore-parallel bars occurring simultaneously (Short, 1991; Ruessink et al., 2003; Walstra et al., 2012). However, in contrast to submerged bars, chenier crests quickly develop to a height around or above MSL, thus emerging during (part of) each tidal cycle. As a result, the most seaward chenier crest cuts off the more landward crest from tidal and wave influences, blocking any further sand supply and effectively stopping its dynamics. This is in agreement with observations by Woodroffe et al. (1983) on the chenier plain in the Firth of Thames, New Zealand.

By using the stratigraphy schematisation in Delft3D to model separate bed layers, we modelled the winnowing process in detail. We showed that even for very low sand content (5%), a chenier can be formed. This agrees with the findings of Nardin and Fagherazzi (2018) that sand availability usually is not the limiting factor in chenier formation (except for extremely low sand contents). This finding explains the presence of cheniers in areas without a nearby source of coarser sediments, e.g. in Demak, Indonesia.

Possibly the largest limitation of our modelling approach is the absence of sand-mud interactions. In our model set-up, a cohesive (mud) and a non-cohesive (sand) fraction were considered independently: the sand fraction is mainly transported as suspended load due to wave asymmetry once a critical bed shear stress based on the Shields curve is exceeded; the mud fraction is transported as a suspended load, once the critical bed shear stress for erosion is exceeded. However, a sand-mud mixture will behave as a cohesive mixture when the mud content is higher than 30% (van Ledden et al., 2004). Such a mixture will typically have a higher critical bed shear stress for erosion (van Rijn, 2020). Furthermore, we assumed a relatively low settling velocity and critical bed shear stress for the mud fraction. Altogether, this means that our model results may overestimate the speed (and extent) at which winnowing takes place.

5 Conclusions

A numerical model (Delft3D) is used to analyse how cheniers develop through wave-induced winnowing and transport. We identify three phases in chenier genesis: (1) winnowing, when the mud is washed out and the upper layer of the sediment becomes increasingly sandy; (2) sand transport, when the sand in the upper layer is transported landward; and (3) crest formation, when the sand culminates at one point, resulting in a rapid heightening of the chenier crest. Winnowing takes place when mud is eroded from the bed and brought into suspension (when $\tau_{\mathrm{cw,max}} > \tau_{\mathrm{cr,e}}$), leaving behind a fine layer of sand. Sand transport takes places when the threshold for the initiation of motion is exceeded (when $v_{\mathrm{eff}} > v_{\mathrm{cr}}$). The onshore sand transport is mainly driven by wave asymmetry, and is supply-limited (directly depending on the winnowing). Crest formation occurs when the peak of the sand transport rate converges at the shoreline, locally generating steep negative transport gradients resulting in rapid sedimentation.

The model study suggests that chenier formation does not require extreme storm conditions. Winnowing and onshore sand transport (phases 1 and 2) already take place under calm conditions, but crest formation (phase 3) requires sufficient sand to be transported nearshore. Under sea breeze conditions, the area where sand transport takes place is too small to supply sufficient sand to develop into a crest, only creating a thin nearshore layer of sand. However, average storm conditions which are exceeded several times per year, do generate sand transport over a sufficiently large spatial scale for a chenier to develop. Calm conditions therefore do not directly lead to chenier development but do result in landward transport of sand (as long as the upper layer of the bed is not depleted) which speeds up the formation of a crest during more energetic periods following that period of calm conditions.

Starting from a well-mixed bed, chenier formation is a slow process (requiring at least 8-10 weeks of uninterrupted storm conditions). Especially the time period associated with winnowing and sand transport (phases 1 and 2) is long, followed by a rapid crest formation (phase 3). The model study reveals that cheniers generally develop quicker for a lower sand content in the bed because the upper bed layers are more quickly depleted of sand. Therefore the maximum sand transport converges more rapidly with the shoreline (onset of crest formation, phase 3). On the other hand, larger tidal amplitudes slow down chenier formation, due to temporal and spatial variability of bed shear stresses and periods of emergence in the region of chenier development.

Appendix A Sediment Transport Formulae in Delft3D

A1 Bed Load Transport

The bed load transport is calculated using the empirical formula of van Rijn (1993):

$$S_b = \begin{cases} 0.006\rho_s w_s D_{50} M^{0.5} M_e^{0.7} & \text{if } v_{\text{eff}} \geq v_{\text{cr}} \\ 0 & \text{if } v_{\text{eff}} < v_{\text{cr}} \end{cases}, \tag{A1}$$

where S_b is the bed load transport (in kg/m/s), ρ_s is the sediment density (in kg/m^3), w_s is the settling velocity for the D_{50} of the sediment (in m/s), and D_{50} is the median diameter of the sediment fraction (in m). M is the sediment mobility number due to waves and currents (see Equation A2) and M_e is the excess sediment mobility number (see Equation A3).

The sediment mobility number, M, is defined as:

$$M = \frac{v_{\text{eff}}^2}{(s-1)gD_{50}}, \tag{A2}$$

and the excess sediment mobility number, M_e, is defined as:

$$M_e = \frac{(v_{\text{eff}} - v_{\text{cr}})^2}{(s-1)gD_{50}}, \tag{A3}$$

where v_{eff} is the effective velocity due to waves and currents (see Equation A4, in m/s), v_{cr} is the critical velocity for the initiation of motion (see Equation A6, in m/s), s is the relative density (see Equation A5) and g is the gravitational acceleration (in m/s^2).

The effective velocity due to waves and currents, v_{eff}, is:

$$v_{\text{eff}} = \sqrt{v_{\text{R}}^2 + U_{\text{on}}^2}, \tag{A4}$$

where v_{R} is the magnitude of the depth-averaged current velocity (in m/s) and U_{on} is the onshore-directed, high frequency near-bed orbital velocity (in m/s), calculated using a modification of the method of Isobe and Horikawa (1982) by Grasmeijer and van Rijn (1998).

The relative density s is defined as:

$$s = \frac{\rho_s}{\rho_w}. \tag{A5}$$

The critical velocity for the initiation of motion is determined based on a parametrisation of the Shields curve (van Rijn, 1993; Soulsby, 1997):

$$v_{\text{cr}} = \begin{cases} {0.19D_{50}}^{0.1} \log_{10}\left(\frac{4h}{D_{90}}\right) & \text{if } D_{50} \leq 0.5 \text{ mm} \\ {8.5D_{50}}^{0.6} \log_{10}\left(\frac{4h}{D_{90}}\right) & \text{if } 0.5 \text{ mm} < D_{50} \leq 2 \text{ mm} \end{cases}, \tag{A6}$$

where h is the water depth (in m) and D_{90} is the sediment diameter (in m) for which 90% of the sediment has a smaller diameter, and is based on the composition of the local sediment mixture. In this case, $D_{90} = 1.5D_{50}$.

The bed load transport S_b consists of a current-driven component, $S_{b,c}$, and a wave-driven component, $S_{b,w}$:

$$S_b = \sqrt{{S_{b,c}}^2 + {S_{b,w}}^2 + 2|S_{b,c}||S_{b,w}|\cos(\varphi)}, \tag{A7}$$

with φ the angle between the current and wave direction. From this equation it follows that the current-driven and wave-driven components, $S_{b,c}$ and $S_{b,w}$ respectively, can be calculated as:

$$S_{b,c} = \begin{cases} \frac{S_b}{\sqrt{1+r^2+2|r|\cos(\varphi)}} & \text{if } r \leq 100 \\ 0 & \text{if } r > 100 \end{cases}, \tag{A8}$$

$$|S_{b,w}| = \begin{cases} r|S_{b,c}| & \text{if } r \geq 0.01 \\ 0 & \text{if } r < 0.01 \end{cases}, \tag{A9}$$

with:

$$r = \left(\frac{|U_{\text{on}}| - v_{\text{cr}}}{|v_{\text{R}}| - v_{\text{cr}}} \right)^3. \tag{A10}$$

A2 Suspended Transport

Suspended transport is described by an advection-diffusion equation. In depth-averaged mode ($\partial/\partial z = 0$) and assuming longshore uniformity ($\partial/\partial y = 0$) this equation reads:

$$\frac{\partial ch}{\partial t} + \frac{\partial Uch}{\partial x} - h\frac{\partial}{\partial x}\left(\epsilon_{s,x}\frac{\partial c}{\partial x}\right) = E - D \tag{A11}$$

where c is the concentration (in kg/m^3), h is the water depth (in m), U is the depth-averaged velocity in x-direction (in m/s), w_s is the settling velocity (in m/s), $\epsilon_{s,x}$ is the horizontal eddy diffusivity (in m^2/s), E is the erosion flux (in kg/m^2/s) and D is the deposition flux (in kg/m^2/s). In Equation A11, the second term gives the advective transport, the third term the diffusive transport and the right hand side represents the source and sink terms (to and from the bed). For cohesive sediment, the erosion and depositional fluxes are calculated with the Partheniades erosion formulation (Partheniades, 1965) and a permanent deposition flux (Winterwerp, 2007):

$$E = M_{\text{ero}} S(\tau_{\text{cw,max}}, \tau_{\text{cr,e}}), \tag{A12}$$

and

$$D = w_s c_b, \tag{A13}$$

where M_{ero} is an erosion parameter (in kg/m^2/s), $S(\tau_{\text{cw,max}}, \tau_{\text{cr,e}})$ is an erosion function (see Equation A14) and c_b is the average sediment concentration near the bed (in kg/m^3).

The erosion function is defined as:

$$S(\tau_{\text{cw,max}}, \tau_{\text{cr,e}}) = \begin{cases} \left(\frac{\tau_{\text{cw,max}}}{\tau_{\text{cr,e}}} - 1\right) & \text{if } \tau_{\text{cw,max}} > \tau_{\text{cr,e}} \\ 0 & \text{if } \tau_{\text{cw,max}} \leq \tau_{\text{cr,e}} \end{cases}, \tag{A14}$$

Here, $\tau_{\text{cr,e}}$ is the critical bed shear stress for erosion (in N/m^2) and $\tau_{\text{cw,max}}$ is the maximum bed shear stress due to current and waves (in N/m^2). This maximum bed shear stress is computed with the parametrisation of Soulsby et al. (1993):

$$|\tau_{\text{cw,max}}| = Z(|\tau_c| + |\tau_w|), \tag{A15}$$

where τ_c is the bed shear stress due to currents (in N/m^2), τ_w is the bed shear stress due to waves (in N/m^2), and Z is a dimensionless parameter.

The bed shear stress due to currents, τ_c, is defined as

$$\tau_c = \frac{g\rho_w U|U|}{C^2}, \tag{A16}$$

where U is the depth-averaged velocity (in m/s) and C is the Chézy coefficient (in m$^{1/2}$/s).

The magnitude of the bed shear stress due to waves alone is defined as:

$$\tau_w = 0.5\rho_w f_w {u_{\text{orb}}}^2, \tag{A17}$$

where f_w is the wave friction factor (defined in Equation A19) and u_{orb} is the peak orbital velocity (in m/s) and can be calculated using linear wave theory:

$$u_{\text{orb}} = \frac{\sqrt{\pi}}{4} \frac{H_{\text{rms}}\omega}{\sinh(kh)}. \tag{A18}$$

Here H_{rms} is the root-mean-square wave height (in m), $\omega = 2\pi/T$ is the wave angular frequency (in s^{-1}) and $k = 2\pi/L$ is the wave number (in m^{-1}) which can be derived from the linear wave dispersion relationship.

The wave friction factor under pure oscillatory flow is calculated following Swart (1974):

$$f_w = \begin{cases} 0.00251 \exp\left[5.21 \left(\frac{A}{k_s}\right)^{-0.19}\right] & \text{if } \frac{A}{k_s} > \frac{\pi}{2} \\ 0.3 & \text{if } \frac{A}{k_s} \leq \frac{\pi}{2} \end{cases}, \tag{A19}$$

where k_s is the Nikuradse roughness height (in m) (which can be derived from the Chézy coefficient, see Equation A21) and A, the orbital excursion length, equals:

$$A = \frac{u_{\text{orb}}}{\omega}. \tag{A20}$$

The Nikuradse roughness height is derived from the Chézy coefficient using the formulation of White-Colebrook:

$$k_s = 12h10^{-C/18} \tag{A21}$$

The dimensionless parameter Z from Equation A15 is defined as:

$$Z = 1 + aX^m(1-X)^n, \tag{A22}$$

with:

$$X = \frac{|\tau_c|}{|\tau_c| + |\tau_w|}. \tag{A23}$$

The value of the parameters a, m and n can be determined through the following expression:

$$\chi = \left(\chi_1 + \chi_2|\cos\varphi|^J\right) + \left(\chi_3 + \chi_4|\cos\varphi|^J\right)\log_{10}\left(\frac{f_w}{C}\right) \tag{A24}$$

where φ is the angle between the current direction and the direction of wave propagation and χ represents a, m or n. The fitting coefficients based on Fredsøe (1984) are used, see Table A1.

Table A1. Fitting coefficients for wave-current boundary layer model, using FR84 (Fredsøe, 1984)

FR84	χ_1	χ_2	χ_3	χ_4
a	-0.06	1.70	-0.29	0.29
m	0.67	-0.29	0.09	0.42
n	0.75	-0.27	0.11	-0.02
J		0.80		

In addition to the suspended transport via advection and diffusion (which in this case is mostly mud transport), there is also suspended sand transport due to wave asymmetry. This component represents the effect of asymmetric wave orbital velocities on suspended sediment transport within about 0.5 m of the bed and can be approximated following van Rijn et al. (2001):

$$S_{s,w} = f_{\mathrm{SUSW}}\gamma U_A S_S, \tag{A25}$$

where f_{SUSW} is a user-defined tuning parameter, γ is the phase lag coefficient ($\gamma = 0.2$), U_A is the velocity asymmetry value (in m/s, see Equation A26) and S_S is the suspended sediment load (in kg/m/s, see Equation A27).

The velocity asymmetry value, U_A, is defined as:

$$U_A = \frac{{U_{\text{on}}}^4 - {U_{\text{off}}}^4}{{U_{\text{on}}}^3 + {U_{\text{off}}}^3}, \tag{A26}$$

and the suspended sediment load, S_S, as:

$$S_S = 0.007 \rho_s D_{50} M_e. \tag{A27}$$

In Delft3D, this transport component is included in the bed load vector, because it does not exhibit the relaxation effects of an advection-diffusion relation (Deltares, 2021).

Acknowledgments

This work is part of the BioManCO project with project number 14753, which is (partly) financed by NWO Domain Applied and Engineering Sciences, and co-financed by Boskalis Dredging and Marine Experts, Van Oord Dredging and Marine Contractors bv, Deltares, Witteveen+Bos and Wetlands International. The BioManCO project is a collaboration between TU Delft, NIOZ and UNDIP and makes use of the framework set up by Building with Nature Indonesia, a programme by Ecoshape, Wetlands International, the Indonesian Ministry of Marine Affairs and Fisheries (MMAF), the Indonesian Ministry of Public Works and Housing (PU) and other partners.

References

Alferink, M. (2022). *Wave transmission through permeable structures in Demak Indonesia* (MSc thesis, Delft University of Technology). Retrieved from `http://resolver.tudelft.nl/uuid:23dc0cc4-9658-44ab-a067-5800a0731853`

Anthony, E. J., Brunier, G., Gardel, A., & Hiwat, M. (2019). Chenier Morphodynamics on the Amazon-Influenced Coast of Suriname, South America: Implications for Beach Ecosystem Services. *Frontiers in Earth Science*, *7*(March), 1–20. doi: 10.3389/feart.2019.00035

Anthony, E. J., Gardel, A., Gratiot, N., Proisy, C., Allison, M. A., Dolique, F., & Fromard, F. (2010). The Amazon-influenced muddy coast of South America: A review of mud-bank-shoreline interactions. *Earth-Science Reviews*, *103*, 99–121. doi: 10.1016/j.earscirev.2010.09.008

Augustinus, P. G. E. F. (1980). Actual development of the chenier coast of Suriname (South America). *Sedimentary Geology*, *26*(1-3), 91–113. doi: 10.1016/0037-0738(80)90007-X

Augustinus, P. G. E. F. (1989). Cheniers and chenier plains: A general introduction. *Marine Geology*, *90*(4), 219–229. doi: 10.1016/0025-3227(89)90126-6

Belperio, A. P., Gostin, V. A., Cann, J. H., & Murray-Wallace, C. V. (1988). Sediment-organism zonation and the evolution of Holocene tidal sequences in Southern Australia. In P. L. de Boer, A. van Gelder, & S. D. Nio (Eds.), *Tide-influenced sedimentary environments and facies* (pp. 475–497). Dordrecht, the Netherlands: D. Reidel Publlishing Company.

Booij, N., Ris, R. C., & Holthuijsen, L. H. (1999). A third-generation wave model for coastal regions: 1. Model description and validation. *Journal of Geophysical Research*, *104*(C4), 7649–7666. doi: 10.1029/98JC02622

Deltares. (2021). *Delft3D-FLOW. Simulation of multi-dimensional hydrodynamic flows and transport phenomena, including sediments. User Manual* (Tech. Rep.). Delft: Author. Retrieved from `https://content.oss.deltares.nl/delft3d/manuals/Delft3D-FLOW_User_Manual.pdf`

Deltares, & BioManCO. (2019). *Sediment analysis of Demak* (Tech. Rep.). Delft: Deltares.

Dougherty, A. J., & Dickson, M. E. (2012). Sea level and storm control on the evolution of a chenier plain, Firth of Thames, New Zealand. *Marine Geology*, *307-310*, 58–72. doi: 10.1016/j.margeo.2012.03.003

Fredsøe, J. (1984). Turbulent boundary layer in wave-current motion. *Journal of Hydraulic Engineering*, *110*(8), 1103–1120. doi: https://doi.org/10.1061/(ASCE)0733-9429(1984)110:8(1103)

Grasmeijer, B. T., & van Rijn, L. C. (1998). Breaker Bar Formation and Migration. In *26th international conference on coastal engineering* (pp. 2750–2758). doi: 10.1061/9780784404119.208

Isobe, M., & Horikawa, K. (1982). Study on water particle velocities of shoaling and breaking waves. *Coastal Engineering in Japan*, *23*, 109–123. doi: 10.1080/05785634.1982.11924340

Lesser, G. R., Roelvink, J. A., van Kester, J. A. T. M., & Stelling, G. S. (2004). Development and validation of a three-dimensional morphological model. *Coastal Engineering*, *51*(8-9), 883–915. doi: 10.1016/j.coastaleng.2004.07.014

Manning, A. J., & Dyer, K. R. (2007). Mass settling flux of fine sediments in Northern European estuaries: Measurements and predictions. *Marine Geology*,

245(1-4), 107–122. doi: 10.1016/j.margeo.2007.07.005

Nairn, R. B., Roelvink, J. A., & Southgate, H. N. (1991). Transition Zone Width and Implications for Modelling Surfzone Hydrodynamics. In B. L. Edge (Ed.), *22nd international conference on coastal engineering 1990* (pp. 68–81). American Society of Civil Engineers. doi: 10.1061/9780872627765.007

Nardin, W., & Fagherazzi, S. (2018). The Role of Waves, Shelf Slope, and Sediment Characteristics on the Development of Erosional Chenier Plains. *Geophysical Research Letters*, *45*(16), 8435–8444. doi: 10.1029/2018GL078694

Otvos, E. G., & Price, W. A. (1979). Problems of chenier genesis and terminology - An overview. *Marine Geology*, *31*(3-4), 251–263. doi: 10.1016/0025-3227(79)90036-7

Partheniades, E. (1965). Erosion and deposition of cohesive soils. *Journal of the Hydraulics Division*, *91*(1), 105–139. doi: https://doi.org/10.1061/JYCEAJ.0001165

Prost, M. T. (1989). Coastal dynamics and chenier sands in French Guiana. *Marine Geology*, *90*(4), 259–267. doi: 10.1016/0025-3227(89)90128-X

Pujos, M., Pons, J.-C., & Parra, M. (2001). Les minéraux lourds des sables du littoral de la Guyane française: bilan sur l'origine des dépôts de la plateforme des Guyanes. *Oceanologica Acta*, *24*(SUPPL). doi: 10.1016/s0399-1784(01)00093-7

Reniers, A. J. H. M., Roelvink, J. A., & Thornton, E. B. (2004). Morphodynamic modeling of an embayed beach under wave group forcing. *Journal of Geophysical Research*, *109*(C01030). doi: 10.1029/2002jc001586

Rhodes, E. G. (1982). Depositional model for a chenier plain, Gulf of Carpentaria, Australia. *Sedimentology*, *29*, 201–221. doi: 10.1111/j.1365-3091.1982.tb01719.x

Rosen, T., & Xu, Y. J. (2011). Riverine sediment inflow to Louisiana Chenier Plain in the Northern Gulf of Mexico. *Estuarine, Coastal and Shelf Science*, *95*(2-3), 279–288. doi: 10.1016/j.ecss.2011.09.013

Ruessink, B. G., Wijnberg, K. M., Holman, R. A., Kuriyama, Y., & van Enckevort, I. M. J. (2003). Intersite comparison of interannual nearshore bar behavior. *Journal of Geophysical Research*, *108*(C8). doi: 10.1029/2002JC001505

Short, A. D. (1991). Macro-Meso Tidal Beach Morphodynamics - An Overview.

Journal of Coastal Research, *7*(2), 417–436. Retrieved from https://www.jstor.org/stable/4297847

Soulsby, R. L. (1997). *Dynamics of marine sands*. London: Thomas Telford. Retrieved from http://www.icevirtuallibrary.com/content/book/100318

Soulsby, R. L., Hamm, L., Klopman, G., Myrhaug, D., Simons, R. R., & Thomas, G. P. (1993). Wave-current interaction within and outside the bottom boundary layer. *Coastal Engineering*, *21*, 41–69. doi: 10.1016/0378-3839(93)90045-A

Soulsby, R. L., Manning, A. J., Spearman, J., & Whitehouse, R. J. S. (2013). Settling velocity and mass settling flux of flocculated estuarine sediments. *Marine Geology*, *339*, 1–12. doi: 10.1016/j.margeo.2013.04.006

Svendsen, I. A. (1984). Wave heights and set-up in a surf zone. *Coastal Engineering*, *8*, 303–329. doi: 10.1016/0378-3839(84)90028-0

Swart, D. H. (1974). *Offshore sediment transport and equilibrium beach profiles* (PhD thesis, Delft University of Technology). Retrieved from http://resolver.tudelft.nl/uuid:057cb136-5f5b-484a-878d-5616fbaeda4e

Tas, S. A. J., van Maren, D. S., Helmi, M., & Reniers, A. J. H. M. (2022). Drivers of cross-shore chenier dynamics off a drowning coastal plain. *Marine Geology*, *445*(106753). doi: 10.1016/j.margeo.2022.106753

Tas, S. A. J., van Maren, D. S., & Reniers, A. J. H. M. (2020). Observations of Cross-Shore Chenier Dynamics in Demak , Indonesia. *Journal of Marine Science and Engineering*, *8*(972). doi: 10.3390/jmse8120972

The WAVEWATCH III Development Group. (2019). *User manual and system documentation of WAVEWATCH III version 6.07* (Vol. Technical Note 333; Tech. Rep.). College Park, MD, USA: NOAA/NWS/NCEP/MMAB.

van Ledden, M., Van Kesteren, W. G. M., & Winterwerp, J. C. (2004). A conceptual framework for the erosion behaviour of sand-mud mixtures. *Continental Shelf Research*, *24*(1), 1–11. doi: 10.1016/j.csr.2003.09.002

van Leussen, W., & Cornelisse, J. M. (1993). The determination of the sizes and settling velocities of estuarine flocs by an underwater video system. *Netherlands Journal of Sea Research*, *31*(3), 231–241. doi: 10.1016/0077-7579(93)90024-M

van Maren, D. S., van Kessel, T., Cronin, K., & Sittoni, L. (2015). The impact of channel deepening and dredging on estuarine sediment concentration. *Conti-*

nental Shelf Research, *95*, 1–14. doi: 10.1016/j.csr.2014.12.010

van Maren, D. S., Winterwerp, J. C., & Vroom, J. (2015). Fine sediment transport into the hyper-turbid lower Ems River: the role of channel deepening and sediment-induced drag reduction. In C. K. Harris (Ed.), *12th international conference on cohesive sediment transport.* Springer. doi: 10.1007/s10236-015-0821-2

van Rijn, L. C. (1993). *Principles of sediment transport in rivers, estuaries and coastal seas.* Amsterdam, the Netherlands: Aqua Publications.

van Rijn, L. C. (2020). Erodibility of Mud–Sand Bed Mixtures. *Journal of Hydraulic Engineering*, *146*(1), 04019050. doi: 10.1061/(asce)hy.1943-7900.0001677

van Rijn, L. C., Roelvink, J. A., & ter Horst, W. (2001). *Approximation formulae for sand transport by currents and waves and implementation in in DELFT-MOR* (Tech. Rep.). Delft, the Netherlands: WL — Delft Hydraulics. Retrieved from `http://resolver.tudelft.nl/uuid:c226bf0a-79d6-4357-80ff-c68c4d5f0416`

Walstra, D. J. R., Reniers, A. J. H. M., Ranasinghe, R., Roelvink, J. A., & Ruessink, B. G. (2012). On bar growth and decay during interannual net offshore migration. *Coastal Engineering*, *60*, 190–200. doi: 10.1016/j.coastaleng.2011.10.002

Winterwerp, J. C. (2007). On the sedimentation rate of cohesive sediment. In J. P. Y. Maa, L. P. Sanford, & D. H. Schoellhamer (Eds.), *Estuarine and coastal fine sediments dynamics: Intercoh 2003* (Vol. 8, pp. 209–226). Elsevier B.V. doi: 10.1016/S1568-2692(07)80014-3

Woodroffe, C. D., Curtis, R. J., & Mclean, R. F. (1983). Development of a chenier plain, Firth of Thames, New Zealand. *Marine Geology*, *53*, 1–22. doi: https://doi.org/10.1016/0025-3227(83)90031-2

Woodroffe, C. D., & Grime, D. (1999). Storm impact and evolution of a mangrove-fringed chenier plain, Shoal Bay, Darwin, Australia. *Marine Geology*, *159*, 303–321. doi: 10.1016/S0025-3227(99)00006-7